This article was published in Applied Catalysis B: Environmental, 154-155, 316-328, 2014
http://dx.doi.org/10.1016/j.apcatb.2014.02.032

Ultraselective low temperature steam reforming of methanol over PdZn/ZnO catalysts—Influence of induced support defects on catalytic performance

Katarzyna Morawa Eblagon[a], Patricia Heydorn Concepción[b], Hugo Silva[a], Adélio Mendes[a,*]

[a] *Faculty of Chemical Engineering, University of Porto, Rua Doutor Roberto Frias s/n, 4200-465 Porto, Portugal*

[b] *Instituto de Tecnologíia Química, Universitat Politecnica de Valencia (UPV-CSIC) , Avenida de los Naranjos s/n, 46022 Valencia, Spain*

* Corresponding author. Tel.: +351 225081695.
E-mail addresses: k.eblagon@fe.up.pt (K.M. Eblagon), pconcepc@upvnet.upv.es (P.H. Concepción), silva.hugo@fe.up.pt (H. Silva), mendes@fe.up.pt (A. Mendes).

Abstract

The influence of the calcination atmosphere of ZnO precursor ($Zn_4(CO)_3(OH)_6 \cdot H_2O$) on the catalytic performance of a series of PdZn/ZnO catalysts was studied for production of H_2 via low temperature (180 °C) direct methanol steam reforming (low temperature-MSR). The catalytic activity and selectivity of PdZn/ZnO were found to be strongly influenced by the calcination atmosphere of ZnO precursor and increased from oxidizing to reducing atmosphere, following the order (O_2 < air < N_2 < H_2). As a result, a very active catalyst was obtained by simply supporting Pd on ZnO calcined in H_2. Further evidence from XPS and TPR analysis indicated that calcination in reducing atmosphere gave rise to a significant increase in the concentration of oxygen vacancies on the surface of ZnO support. Thus, the superb performance of the best catalyst was attributed to the defect chemistry of ZnO support; mainly to the amount of oxygen vacancies present in the interface region, which act as additional active sites for water adsorption and subsequent activation. In addition, the formation of CO was drastically suppressed by replenishment of oxygen vacancies on ZnO support. Thus, it is clear that the abundance of specific active sites on PdZn/ZnO catalyst is strongly influenced by the preparation route of the ZnO support. Additionally, the PdZn alloy was discovered to be unstable under prolonged exposure to CO atmosphere and the stability test under methanol steam reforming conditions showed a 24% drop in conversion over 48 h testing period. This phenomena can have detrimental effect on the performance of this type of catalytic systems in continuous prolonged duty cycle time on-stream.

1. Introduction

Hydrogen will surely contribute to the world energy market in the mid-term to long-term future [1,2]. However, one of the major obstacles of "Hydrogen Economy" is finding a feasible method to store and distribute sufficient amount of hydrogen mainly for transportation sector [3]. Recently, reformers that can extract hydrogen from fuels gained increased research interest due to the fact that they can be integrated directly with polymer electrolyte fuel cell (PEMFC). As a result, high purity H_2 can be produced *in situ* on board of the vehicle via well-established steam reforming of alcohols from biomass, or hydrocarbons [4]. In this regard, methanol is a promising hydrogen carrier candidate for the future [5] mainly because it has high H to C ratio, low chemical energy bond [6] and can be produced either by reduction CO_2 or from diverse bio-based resources [7].

Methanol steam reforming (MSR) is accompanied with side- reactions such as: methanol decomposition (MD), water gas shift (WGS) and reversed water gas shift (RWGS) [8,9]. The extent of these processes depends on the feed composition, reaction conditions and the catalyst used. Due to MD and RWGS reactions being always present, the reformate gas inevitably contains CO contaminant which even in trace levels can poison the PEMFC anode [2,10]. For example, high temperature PEMFC (HT-PEMFC) using polybenzimidazole membranes working at 180 °C can only tolerate a maximum of 1–2% CO in the anode feed [11]. One approach to decrease the amount of produced CO is to lower the temperature of MSR to the point at which MD is suppressed and WGS reaction is favored due to the thermodynamics of these processes [9]. A catalyst able to work efficiently at lower temperatures is also cost- effective and desirable taking into consideration the integration between the endothermic MSR and exothermic PEMFC operation. Furthermore, low operating temperatures are beneficial for applications as power supplies for small portable devices, where heat and space management are of primary concern [12]. However, the development of a suitable catalytic system promoting both endothermic MSR and exothermic WGS at reasonably low temperatures (below 200 °C) remains a challenge.

Cu based catalysts are typically used for MSR due to their relatively low cost, very high activity and low CO production at temperatures below 300 °C [13]. Thus, several catalyst formulations were studied, such as binary compositions; Cu/ZnO, Cu/SiO_2, Cu/CeO_2 [4], commercially based Cu/ZnO/γ-Al_2O_3 and its variations with added promoters; Cu/ZrO_2/γ-Al_2O_3, Cu/Cr/γ-Al_2O_3 [2] or CuTiP/γ-Al_2O_3 [6]. More recently CuZnGaOx [12] and CuZn catalyst promoted by rare earth metals such as Tb and Pr [14] were reported to have high activity at low temperature MSR. Nevertheless, Cu based catalysts have some considerable drawbacks which include pyrophoricity and easy deactivation due to thermal instability [7,15] or coke formation [13]. Additionally, these catalysts are sensitive towards condensing steam [6], which results in declining activity and mechanical integrity of the catalytic system under duty cycle conditions [11].

The search for a more suitable catalyst for MSR has led to a discovery that the inherent high selectivity of Pd catalyst towards MD can be drastically switched to high selectivity in MSR by simply changing the material of the support [16]. Apparently, Pd supported on hard-to-reduce oxides M_xO_y (M= Si, Al, Mg, Zr, Pr, Ce, La) is highly selective to MD [17,18]. On the other hand, Pd supported on easily reducible oxides such as ZnO, Ga_2O_3 or In_2O_3 becomes active and selective in MSR. Unusual behavior of these Pd based catalysts was attributed to a formation

of alloys PdMe (Me = Zn, Ga, In) upon proper reductive pretreatment, leading to a bifunctional synergism between intermetallic and oxide species which is necessary for a good catalytic performance in MSR [19,20]. In addition, the *in situ* partial oxidation of PdZn nanoparticles was observed recently to result in the formation of a large interface between the intermetallic PdZn and small ZnO patches, which improved the selectivity to CO_2 in MSR [20]. It is thus evident that the performance of Pd/ZnO catalyst is not only dependent on the chemical composition or size of the active species, but it is also governed by the type of active sites present on its surface [21]. Moreover, there was an indication that addition of Zn to Pt or Pd altered the barriers for C–H cleavage and thus changed the stability of various intermediates in MSR [22]. The PdZn/ZnO interface was found to increase water activation at lower temperatures, therefore promoting CO_2 selectivity [23]. However, the role of ZnO in the performance of PdZn/ZnO is not yet fully understood.

ZnO is an anisotropic oxide which contains intrinsically unstable polar facets with point defects that compensate for a surface dipole moment and non-polar facets which exhibit densely packed Zn and O atoms that are electrically neutral [24]. In addition, stronger electronic interaction and facile PdZn alloy formation was reported on Pd supported on ZnO with majority of polar facets exposed on the surface. Furthermore, it was shown previously that the exposure of ZnO to atmospheric pressure of H_2, can change the concentration of the Schottky defects mainly that of oxygen vacancies [25]. In addition, the creation of defects through reduction modifies the d-band states of a reducible metal oxide (such as ZnO) which changes the interaction with the adsorbates [26]. As a result, it can be expected that the increased concentration of oxygen vacancies in ZnO support might improve the performance of the PdZn/ZnO catalyst at low temperature MSR. With this regard, the present work will be focused on the performance of PdZn alloys supported on the ZnO calcined in N_2, O_2, air and H_2 in low temperature MSR. The catalytic results will be compared to the performance of PdZn sup- ported on commercial ZnO (Sigma–Aldrich). The aim is to provide an insight into the influence of the active sites present on the sur- face of ZnO support on the activity and selectivity of the PdZn/ZnO catalytic system. Moreover, thorough catalyst characterization was carried out to gain a better understanding of the key parameters controlling the performance of PdZn/ZnO catalysts for low temperature MSR. Thus, the extent of synergetic interaction between PdZn and various ZnO was studied using analytical techniques such as X-ray Diffraction (XRD), Temperature Programmed Reduction (TPR) and X-ray Photoelectron Spectroscopy (XPS). Selected catalysts and ZnO supports were additionally characterised by high resolution transmission electron microscopy (HRTEM) and scanning electron microscopy–

energy dispersive X-ray spectroscopy (SEM-EDX). The active sites and the stability of PdZn/ZnO catalysts was characterised by CO absorption IR DRIFT spectroscopy. Finally, the stability test of the most active catalyst was carried out to access its long term performance under prolonged exposure to methanol steam reforming conditions.

2. Experimental

2.1. *Hydrothermal method of ZnO preparation*

All the reagents were purchased from Sigma–Aldrich and were used without any pretreatment. The ZnO supports were obtained following a conventional hydrothermal synthesis [27]. $Zn(CH_3COO)_2$ was used as a Zn^{2+} precursor, $CO(NH_2)_2$ as precipitant and P123 Pluronic block copolymer as a surfactant. In a typical hydrothermal synthesis; 1.1 g of $Zn(CH_3COO)_2$, 6 g of urea and 3 g of P123 were dissolved in 100 mL of distilled water. Subsequently, the pH of the solution was fixed at 5.0 using CH_3COOH and the mixture was left to homogenize at ambient conditions for 2 h. After a homogenous mixture was obtained, the solution was sealed in a hydrothermal teflon lined reactor and heated in a laboratory oven at 90 °C for 24 h to ensure the complete precipitation of zinc carbonate. Subsequently, the obtained solid product was filtered and washed several times with distilled water and dried overnight at 90 °C in air in an oven. The final step of the preparation of ZnO supports was the calcination of the prepared precursor at 370 °C, with a heating rate of 4.2 °C/min in a flow (200 mL/min) of a selected gas (H_2, O_2, air, N_2) and with a dwell time of 0.5 h. The prepared ZnO supports are hereafter referred as: ZnO H_2—ZnO calcined in H_2; ZnO N_2—ZnO calcined in N_2. ZnO COM is a ZnO commercial support (Sigma–Aldrich), etc.

2.2. *Synthesis of PdZn/ZnO catalysts*

The 4.7 wt % PdZn/ZnO catalysts were prepared following a standard wet impregnation technique, using hydrothermally pre- pared ZnO supports (Section 2.1) and ZnO commercial support (Sigma–Aldrich, ZnO nanopowder) for comparison. In a typical procedure, the appropriate amount of ZnO support was wetted by 10 mL of chloroform to prepare a slurry. Subsequently, a solution of a calculated amount of palladium acetate (Sigma–Aldrich, reagent grade 98%) in 5

mL of chloroform was added dropwise to the slurry of the ZnO support under vigorous ultrasonic treatment. The sol- vent was then dried out at ambient conditions under continuous magnetic stirring while placed in a fume hood. PdZn alloy formation is necessary to obtain good catalytic activities in MSR, thus the catalyst reduction temperature was optimized by monitoring various reduction temperatures using an on-line XRD technique. The optimum temperature of PdZn alloy formation was chosen at 400 °C in H_2 flow (200 mL/min), with a heating rate of 4.2 °C/min and a dwell time of 2 h.

2.3. *Physicochemical characterization of supports and catalysts*

The physicochemical properties of ZnO supports were characterised using a variety of methods. The morphology and qualitative composition was obtained from SEM images and EDX, respectively. The SEM micrographs were recorded using a high resolution (Schottky) environmental scanning electron microscope with X-ray microanalysis and backscattered electron diffraction pattern analysis working at 20 kV. Shape and sizes of the particles were obtained using image analysis software (ImageJ). The average diameter of the ZnO assemblies was obtained measuring at least 100 particles from three different regions of each of the samples. The composition of the supports was studied at a magnification of about 600*k*. Four different areas of each of the samples were examined by EDX analysis with working distance set at 25 mm, dead time 50% and a process time of 6 min.

The crystallographic characterisation of ZnO supports was obtained using the XRD technique. The XRD pattern of the selected samples was collected using a Philips PW1729 diffractometer operating in Bragg-Brentano focusing geometry and using Cu $K\alpha$ radiation at wavelengths Cu $K\alpha 1$ = 154.06 pm and Cu $K\alpha 2$ = 154.439 pm. The data was collected at 2θ angles (20–70°), with a step size of 0.02°, step speed of 0.5°/min and at 1.25 s per step. The obtained X-ray scans were compared to those of standard database and the phases were assigned comparing the data available in literature.

BET surface area of ZnO supports was measured following a standard procedure, obtaining N_2 11 point adsorption isotherms at 77 K. Prior to the measurements, the samples were outgassed in vacuum at 300 °C for 2 h.

The neat ZnO supports and as-prepared PdZn/ZnO catalysts were characterised using a TEM CM 20 (accelerating voltage 310 and 208 kV at nominal magnification) and a HRTEM JEOL 2010 (accelerating voltage 600 kV, at

±

nominal magnification 590 kV). For determination of a particle size distribution, not less than 100 particles from different areas of the sample were measured, using the Scandium software from Olympus Soft Imaging Solutions. The determination of the lattice d-spacing was carried out using high resolution micrographs of the lattice, taking at least five measurements from different areas of the sample. The estimated error of the measurements was 0.01 nm.

The interaction between metal and support in PdZn/ZnO calcined at various atmospheres was probed using X-ray photo- electron spectroscopy (XPS). The XPS analysis was performed using a Kratos AXIS Ultra HSA, with VISION software for data acquisition and CASAXPS and XPSPeak 41 software for data analysis. The analysis was carried out with a monochromatic Al Kα X-ray source (1486.7 eV), operating at 15 kV (90 W), in FAT mode (Fixed Analyser Transmission), with a pass energy of 40 eV for regions ROI and 80 eV for survey. Data acquisition was performed with a pressure lower than $1.0x10^{-6}$ Pa using a charge neutralization system. The modelling of the spectra was performed using peak fit- ting with Gaussian–Lorentzian (80%) peak shape and Shirley type background subtraction.

The TPR-curves were measured using a quartz flow-through apparatus. Consumption of H_2 was obtained using a Balzers GAM-415 quadrupole mass spectrometer. Hydrogen response was calibrated by pulsing 1 mL of 3% H_2 in argon and measuring the corresponding response. TPR-conditions: H_2/Ar (3 vol%), flow 20 mL/min, heating rate 3 °C/min in the temperature range 30–600 °C.

The nature of the Pd species and the type of active sites present in the prepared PdZn/ZnO catalysts was further characterised by CO-chemisorption IR-DRIFT analysis. The IR-DRIFT analysis was carried out using powder catalyst. The spectra of adsorbed CO were recorded at room temperature (25 °C) with a Nexus 8700 FTIR spectrometer using a DTGS detector with 4 cm^{-1} resolution. An IR cell allowing *in situ* treatments under controlled gas atmosphere and temperature was connected to a vacuum system with gas dosing facility. For IR studies the samples were pressed into self-supported wafers and diluted in ZnO (Sigma–Aldrich) using previously optimised weight ratios. The samples were treated at 300 °C in a 5% H_2 in N_2 flow (15 mL/min) for 2 h followed by evacuation at 10^{-4} mbar at 350 °C for 1 h. After the activation procedure, the samples were cooled down to 25 °C under dynamic vacuum conditions followed by CO dosing at increasing pressure (0.4–15 mbar). Several IR-DRIFT spectra were recorded with increasing exposure time, until no further changes were observed in the spectra indicating full CO saturation of the surface.

The amount of Pd in the samples was determined with an ICP- OES (Vista RL, Varian) after matrix-matched calibration. Not more than 5 mg of the sample was dissolved in 2 mL of aqua regia. Finally, the solutions were diluted in 50-mL volumetric flasks and the analysis was carried out.

The number of surface Pd sites was quantified by CO pulse chemisorption experiments which were conducted using a Micromeritics AutoChem II 2920 analyzer. Catalysts (typically 0.3–0.5 g) were loaded in a quartz tube that was placed in the built- in furnace. The temperature in the catalyst layer was controlled using a type-K thermocouple and the flow of gasses was regulated by a built-in mass flow controllers. The catalysts were typically purged with dry helium at 100 °C for 1 h, followed by reduction in 5% H_2/Ar (flow rate 50 mL/min) at 400 °C for 2 h and then it was cooled down to 50 °C. Subsequently, the cleaned sample was exposed to pulses of 0.5-mL CO until five consecutive pulses yielded identical signal areas. The dispersion of Pd was estimated from the ratio of the number of moles of surface Pd atoms to the total number of moles of Pd atoms present in the catalyst.

2.4. *Catalytic tests*

The catalytic activity tests of MSR were performed in a fixed bed reactor at pressures between 1 and 1.6 bar, with the following experimental conditions: steam/methanol molar ratio of 1.5 and a contact time of W/F_0 = 83 kg mol^{-1} s^{-1} (where W is the mass of the catalyst, 200 mg and F_0 is the flow rate of methanol). The stainless steel microreactor was placed in an electrically heated furnace and the temperature was controlled inside the furnace as well as in the catalytic bed using a K-type thermocouple inserted into the catalytic bed. Argon was used as carrier gas and the flow of reactants was controlled by mass flow meters and the gas products were analysed by an online mass spectrometer. The concentration of CO (ppm) in the products was measured directly using an on-line CO analyser (reading error 2 ppm). An average of at least 10 measurements was taken to reduce the reading error. Prior to the catalytic test, the catalyst was pre-treated *in situ* for 2 h by heating up to 200 °C in a stream of Ar (30 mL/min). Subsequently, the hydrogen gas was switched on and the final stream consisted of 70% H_2/Ar. Finally, the catalyst was cooled down to 180 °C and the reaction mixture was introduced. An average of four measurements spaced by 15 min was taken to assure that a stable state of the catalyst performance was reached.

3. Results and discussion

3.1. *Structural and surface characterisation of ZnO supports*

The hydrothermally prepared ZnO supports showed significantly higher values of BET surface area in comparison to ZnO COM. The BET surface area results are gathered in Table 1. Within in- house made samples, higher surface areas were obtained for ZnO supports calcined in oxidative atmospheres. Larger BET surface area after calcination in air/O_2 than in N_2 were previously observed in case of other oxides [28].

The difference in the surface area obtained with different calcination atmospheres can be linked to the changes in mechanism of thermal decomposition of the precursor with the surrounding atmosphere, where the presence of oxygen increases the formation of highly porous structures due to additional burn out of the material.

The representative XRD patterns of the precursor and ZnO supports studied are shown in Fig. 1. The XRD peaks of the solid samples before calcination were characteristic of $Zn_4(CO)_3(OH)_6$ H_2O (JCPDS Card No.11-0287). After calcination, the diffraction peaks in the pattern (see Fig. 1) were indexed to the hexagonal (wurtzite) ZnO phase (Joint Committee on Power Diffraction Standards card 36-1451). The diffraction peaks at 2*θ* of 31.5°, 34.2°, 36.0°, 47.3°, 56.4°, 62.6°, 65.6°, 67.7°, 68.8° were ascribed to the diffractions from the following ZnO planes: (1 0 0), (0 0 2), (1 0 1), (1 0 2), (1 1 0), (1 0 3), (2 0 0), (1 1 2) and (2 0 1) (29), respectively.

It is noted that the XRD patterns for all of the synthesized ZnO supports closely resembled that of bulk ZnO (Zn COM), regardless the type of gas used during calcination step. However, a typical diffraction peak broadening related to the actual size of the crystallites in a direction normal to the diffracting plane was observed in case of the hydrothermally prepared ZnO supports. This broadening together with a small shift towards higher 2*θ* values can be a result of the difference in shape of these crystallites as compared to the ZnO COM [25].

The reactions of Bronsted acids such as methanol are structurally dependent reactions [30] and more active PdZn catalysts were previously obtained when PdZn was supported on ZnO with (0 0 2) polar facets exposed [31]. With regards to these findings, the anisotropy of the ZnO supports studied in the present work was compared using the relative ratio of intensity of XRD diffraction peaks of non-polar to polar facet (1 0 0)/(0 0 2), according to the method proposed by Tsang et al. [32]. Thus, a lower relative ratio of (1 0 0)/(0 0 2) suggests higher exposure of polar planes, whereas a higher ratio of (1 0 0)/(0 0 2) suggests growing of the crystal along the c-axis [0 0 0 1] direction and a high proportion of non-polar

facets. The obtained (1 0 0)/(0 0 2) XRD ratios for ZnO supports are compared in Table 1. As it can be seen from these results, the ratio of relative peak intensities of the studied supports was in the range of 1.13–1.59. It is noted that this is rather small variation, which indicates only small differences in the amount of exposed polar facets among these ZnO supports. As a matter of fact, the aspect ratio of these ZnO supports is very similar. The ratio (1 0 0)/(0 0 2) obtained for commercial ZnO was 1.2 which agrees well with the reported values [32]. Thus, the lowest exposure of polar facets was obtained in the samples calcined in oxidative atmospheres, as it can be seen in Table 1. The representative HRTEM images of ZnO H_2 and ZnO COM are shown in Fig. 2.

The morphology of the obtained ZnO supports calcined at various atmospheres was additionally examined by SEM and the resulting micrographs are shown in Fig. 3 together with the related particle size distributions. In general, low magnification images of the ZnO supports, regardless of the calcination atmosphere, showed mostly uniform spherical particles with diameters in the micron range. However, careful examination disclosed that the morphology of ZnO was strongly affected by the type of gas used during calcination step.

A closer look at a single particle showed that the ZnO O_2 support (see Fig. 3A and B) contained mostly round flower-like self-assemblies of thin highly porous nanosheets with a mean diameter of 16.8 μm. The magnified SEM image of the same sample revealed that the nanosheets were self-assembled leaving large voids between each other. In addition, the structure of the nanosheets contained very disordered multiple pores. Thus, high potential for adsorption of gaseous reactants could be anticipated on these ZnO supports due to the structure of the composing nanosheets. The coarse structure of these nanosheets can be attributed to a fast water removal from the precursor. Similar nanoflower assemblies of ZnO were obtained in hydro- thermal synthesis and calcination in air [33]. On the contrary, highly magnified SEM images of ZnO H_2 sample (Fig. 3C and D) revealed that the microspheres in this case were constructed by highly ordered and very short multilayer nanosheets that were closely packed together to form a nanoball-like porous structure. In addition, in ZnO H_2 support, the nanosheets were thicker (60 nm

in width) as compared to nanosheets of ZnO O_2. The mean particle size of ZnO H_2 (see Fig. 3F) was 15.1 μm, which taking into consideration the standard deviation is very similar to the size of the particles of ZnO O_2. The morphology of sample ZnO N_2 closely resembled that of ZnO H_2 with a mean particle size of 13.1 μm. On the other hand, the morphology of ZnO air strongly resembled that of ZnO O_2, with a mean particle diameter of 15.7 μm. Therefore, in general it can be concluded that calcination of zinc carbonate dihydrate precursor in oxidizing atmospheres (O_2, air) results in the nanospheres/nanoflowers assemblies consisting of a flower-like structure. This structure was constructed from highly porous long nanosheets that were joined together incorporating big voids between them. Such morphology resulted in a higher specific surface area. On the other hand, if the calcination was done in a reductive or inert atmosphere (H_2 or N_2) the spherical nanoballs were produced with short and densely packed nanosheets. These ZnO nanoballs had lower BET surface area than the ZnO supports calcined in oxidizing atmospheres. On the other hand, the size of ZnO particles obtained by hydrothermal method was very similar, regardless of the calcination atmosphere used. In comparison, ZnO COM had faceted crystallites that had prevalent morphology of nanorods with approximate dimensions of 80–100 nm in length and 20 nm in width (results not shown) and a very low BET sur- face area (listed in Table 1). Thus, in spite of the similar aspect ratio and polarity, the morphologies of the studied ZnO supports significantly differed from each other. Noteworthy, EDX analysis of the synthesized ZnO supports and ZnO COM agreed well with the XRD results and showed neat ZnO phases without any impurities.

3.2. *Physicochemical characterization of PdZn/ZnO catalysts*

It was considered of interest to study the possible influence of the morphology of ZnO support on the onset temperature of PdZn alloy formation. Thus, the reduction of selected samples was followed by on-line XRD measurements in the temperature range (30–400 °C) and the formation of PdZn alloy was confirmed in all cases, regardless of the type of ZnO support present. The representative XRD pattern of PdZn/ZnO COM is shown in Fig. 4. In all studied supports, only a very broad peak in the region of $2\theta = 40.2°$ belonging to Pd^0 was observed up to 250 °C, which indicates a small particle size. However, this diffraction peak clearly disappears at higher reduction temperatures. It is thus possible that the amount of remaining Pd^0 is below detection limit of the XRD technique, or that the formation of PdZn alloy was completed. As evidenced in Fig. 4, the beginning of alloy formation took place at around 300 °C, which was accompanied by the appearance of the diffraction peaks at $2\theta = 41°$ and 43.9° that are close to the values ascribed to PdZn alloy [34]. Upon further heating, the

crystallinity and particle size of PdZn alloy increased, which was represented by narrowing of these peaks. Similar patterns were obtained for the samples supported on ZnO calcined in H_2, O_2, air and N_2. Based on these results, 400 °C was selected in the present work as an optimum reduction temperature. Overall it was concluded that the onset of PdZn alloy formation was not affected by the morphology of the ZnO support. Lattice fringes of 0.28 nm were measured from HRTEM micro- graphs for ZnO O_2, ZnO H_2 and ZnO COM which can be attributed to the exposure of a ZnO non-polar (1 0 0) plane [29] which is in agreement with the XRD findings. The formation of PdZn alloy under reduction atmosphere in all of the samples was also further supported by the lattice spacing measurements from HRTEM micrographs. A representative HRTEM image of PdZn ZnO H_2 is shown in Fig. 5. As it can be seen in Fig. 5 left, a lattice spacing of 0.22 nm was obtained for the nanoparticle, which matches the value reported for PdZn alloy (1 1 1) [35]. It should be noted, that the lattice fringes of the particles in the range of 3–4 nm were easily obtained, however measuring d-spacings of smaller particles also present in the samples was difficult due to the contrast from the support. Therefore, we have examined more closely selected area of sample PdZn ZnO COM (see Fig. 5, left) that contained the highest average particle size. The image revealed the lattice spacing of the smaller particle (on the left side of Fig. 5) to be 0.23 nm. This result can suggest the presence of Pd (1 1 1), which possesses lattice spacing slightly higher as compared to that of PdZn alloy in accordance with literature findings [35]. It should be underlined that due to the difference in lattice spacing between PdZn and Pd being not more than 3% [35], the phase of these small particles in our case could only be conclusively identified as Pd by joined results from HRTEM, TPR, XPS and CO adsorption-DRIFT analysis described later in this work. A representative lower magnification HRTEM image of the same sample together with the corresponding particle size distribution is shown in Fig. 6. Similarly to these results, the HRTEM analysis of the remaining PdZn/ZnO catalysts, showed finely dispersed particles with no visible agglomeration, regardless of the calcination atmosphere of ZnO precursor. The mean diameters obtained from HRTEM images of PdZn supported on hydrothermally synthesized ZnO were in the range of 2.1 nm to 3.4 nm, which is significantly lower than the mean diameter of the PdZn supported on ZnO COM (8.8 nm). The sizes of the particles are gathered in Table 2. A clear influence of the morphology of ZnO support was observed on the crystallization of PdZn alloy, leading to changes in size of the nanoparticles. In general, smaller particles would be expected on the higher surface area supports, mainly due to higher Pd dispersion and thus longer diffusion distances between neighboring PdZn and decreased sintering of these particles. Nevertheless, no clear trend was observed between the particle size and the surface area of ZnO support in the studied catalysts.

3.3. *Methanol steam reforming*

A good catalyst for low temperature MSR should provide high water and methanol conversions to hydrogen and carbon dioxide while minimising occurrence of any side-reactions. The prepared PdZn alloyed catalysts immobilized on ZnO calcined under various atmospheres were tested for activity and selectivity in MSR at 180 °C using an in-house built MSR set-up as described in the Experimental section. The results of the catalytic activity and selectivity expressed by CO concentration in ppm, are gathered in Table 2 and compared to PdZn alloy supported on ZnO COM. The BET surface area of ZnO supports and their polarity can be found in Table 1.

It was rather surprising to find that the catalytic activity was independent from the BET surface area of ZnO support (compare Table 1 with Table 2), which is in contrast with the literature reports [27]. On the other hand, selectivity to CO was higher for PdZn catalysts supported on higher surface area ZnO, which were calcined in oxidizing atmosphere. This result can be associated with the apparently lower reducibility of high surface area ZnO supports. Moreover, the selectivity to CO was found to be inversely proportional to the activity for the PdZn supported on hydrothermally obtained ZnO supports (excluding PdZn/ZnO COM). Lower selectivity to CO was achieved by PdZn supported on ZnO with higher exposure of polar facets which is in agreement with the literature [25]. However, no direct trend was established between increased polarity of ZnO and activity of the PdZn/ZnO catalysts, which can be explained by the fact that the range of the polarities studied was very narrow. Additionally, smaller PdZn alloy particles obtained on hydrothermally produced ZnO displayed better activity per gram of metal than their bigger counterparts supported on ZnO COM. However, in order to account for the particle size differences between PdZn ZnO H_2 and PdZn ZnO COM, the TOF of these samples was compared and the results are gathered in the supplementary material. The amount of active sites was obtained by CO pulse chemisorption taking into consideration the similar amount of PdZn alloy present on the surface of these catalysts, as showed later in the paragraph describing XPS results of the present work. Similar extent of alloy present is essential in case of this comparison, because the presence of Zn in Pd decreases the amount of chemisorbed CO and therefore alters the Pd:CO stoichiometry, leading to false number of measured active sites on the catalyst [46]. The TOF of PdZn ZnO H_2 was 1.01 s^{-1} and that of PdZn ZnO COM was 0.71 s^{-1}, which is in the range of the values reported in the literature for similar systems [16]. These results show that independently of the particle size, the most active catalyst was obtained by supporting PdZn on ZnO calcined in reductive atmosphere.

Nevertheless, the greatest differences in performance could be assigned to differences in calcination atmosphere of ZnO precursor (H_2, O_2, N_2, air). As it can

be clearly seen in Table 2, the activity of PdZn/ZnO catalysts increased with calcination atmosphere from oxidative (O_2) to reducing (H_2). It should be underlined that over twofold increase in activity was achieved by supporting PdZn on ZnO H_2 as compared to ZnO O_2. Moreover, the selectivity to CO dropped significantly on the PdZn supported on ZnO calcined in N_2 and H_2 as compared to PdZn supported on ZnO calcined in oxidative atmospheres. The decrease in CO production can be a result of more efficient water activation in these supports, prerequisite for CO_2 selective catalyst in MSR [24]. Overall, the anticipated exceptional increase in activity and selectivity of PdZn supported on ZnO calcined in H_2 atmosphere can be associated with the presence of different active sites, mainly oxygen defects on the surface of the support of this catalyst, which alter the adsorption process of substrates and intermediates during low temperature MSR. It is clear that the difference in catalytic performance as a result of the calcination atmosphere of ZnO showed cannot be attributed to a difference in particle size of the PdZn alloy, as virtually the same particle sizes were obtained in this family of catalysts, regardless of the calcination atmosphere of ZnO. As it was mentioned before, significantly higher size of PdZn particles was noted on the ZnO COM, which can be attributed to the difference in morphology of the ZnO support.

Oxygen vacancies present on the surface of an oxide catalyst are important for several catalytic reactions [31]. However, generally the amount of oxygen vacancies is expected to be higher in ZnO with higher exposure of polar facets, because they are formed to counterbalance the large surface dipole moment [24]. The vacancies can also be created on the non-polar facets of the crystal by treatment in reductive atmosphere, given the right reaction conditions. Much higher conductivity has been previously reported for ZnO materials calcined in oxygen poor atmospheres, which was attributed to a reversible removal of the oxygen atoms from the ZnO lattice and releasing free carriers [37]. Thus, it is likely that the outstanding performance of the PdZn/ZnO H_2 catalyst in the present work is a result of a higher concentration of oxygen vacancies that are produced according to Eq. (1) [37], even though the exposure of polar facets on this support is not the highest in this work (see Table 1)

$$2O_i^{2-} \leftrightharpoons O_2 + 4e^- \qquad (1)$$

These oxygen defects in ZnO create additional active sites to the ones existing on PdZn and on PdZn/ZnO interface, which are responsible for water adsorption. Such a synergy drastically increases the activity of the catalysts at low temperature MSR. Additionally, the improved water activation increases the selectivity towards CO_2 by decreasing the activity of PdZn/ZnO in MD. On the other hand, when the ZnO precursor is calcined in oxidative atmospheres, the

surplus oxygen is able to enter the interstitial sites of ZnO and push the interstitial oxygen atoms back into the lattice, or fill in the existent oxygen vacancies. Thus the amount of V_O–O_i pairs formed decreases. As a result, less available active sites are present on the surface of ZnO leading to poorer catalytic performance. Noteworthy, further evidence had to be obtained to support this speculation.

3.4. XPS study of oxygen vacancies in ZnO supports

XPS is a very useful technique to investigate the chemical and electronic properties of the heterogeneous catalysts. Particularly, the presence of defects in the structure of ZnO can cause changes in chemical bonding resulting in the shifts of binding energy (BE) of the elements in XPS [36]. Thus, the XPS spectra of Pd 3d, Zn 2p, O 1s and C 1s were recorded for selected catalysts and a representative ZnO H2 support. A general XPS survey spectra of all of the catalyst samples showed Pd, Zn, C and O throughout the experiments. With the goal to investigate the abundance of the oxygen vacancies on the PdZn supported on various ZnO supports, the electronic state of the O 1s XPS peak was firstly analysed in higher resolution. A resulting comparison of XPS spectra of oxygen 1s region of the PdZn/ZnO H2 and PdZn/ZnO O2 is shown in Fig. 7. In all cases studied, the obtained O1s asymmetric peak was coherently fitted with three components in agreement with previously reported studies [38]. Accordingly, the oxygen species on the lowest side of the O 1s spectrum labelled as Oa can be attributed to Zn-O bonds of highly crystalline ZnO. The component with the medium BE (labelled Ob) can be assigned to O^{2-} ions in oxygen deficient areas of the ZnO lattice. The changes in intensity of this component mirror the variation in the concentration of oxygen vacancies in ZnO support. In addition, the highest BE peak labelled Oc is associated with adsorbed OH groups on the surface of ZnO. These groups most likely originate from dissociation of adsorbed water on ZnO, which was produced during reduction of PdO [39].

The BE and composition of O 1s spectra of the representative catalysts and ZnO H2 support are gathered in Table 3. As indicated by the results, the highest amount of vacancies (Ob) was found in PdZn ZnO H2. Over 52% of the total oxygen species present on the surface of this catalyst was associated with oxygen defects. On the other hand, the lowest amount of oxygen vacancies was found in PdZn ZnO COM. Moreover, the PdZn supported on ZnO COM had the highest relative concentration of stoichiometric oxygen (Oa) which agrees well with the XRD result (see Fig. 1), showing that ZnO COM had a more crystalline nature than the hydrothermally produced counterparts. In addition, a small shift towards lower values of the BE of oxygen can be noted in case of the most active catalyst as compared to other samples (see Table 3). This can suggest that the electrons are easier to be excited in ZnO H2 due to the significantly higher mobility of interstitial charge

associated with oxygen vacancies. A similar shift of BE of O 1s was previously reported for Cu supported on polar ZnO and was linked to the presence of defects in the ZnO support [21]. Further, as shown in Table 3, the composition of O 1s peak in ZnO H_2 did not change significantly upon addition of Pd and subsequent PdZn alloy for- mation via reduction in H_2. However, a shift of BE towards higher values was observed in PdZn ZnO H_2 as compared to pure support ZnO H_2 (Table 3), which can be attributed to the electronic inter- action between PdZn and support. The electronic synergy leads to a lower charge concentration and thus a higher oxidation state of oxygen.

With regards to the chemical state of Zn in PdZn/ZnO catalysts, the XPS spectra of Zn 2p and Auger Zn LMM peaks were also analysed. The representative XPS spectra of Zn $2p_{3/2}$ of PdZn ZnO COM is shown in Fig. 8. The obtained asymmetric Zn peak could be fitted with two components. Thus, two Zn species coexisted in all of the analyzed catalysts. The lower binding energy was assigned to metallic Zn and the higher BE was assigned to oxidized Zn [40,41]. Similar XPS spectra were obtained for the other studied catalysts.

Different amount of oxygen vacancies in ZnO supports was also confirmed by studying the Auger line of Zn LMM. The BE of Auger Zn LMM is generally more sensitive to the chemical environment [38]. As shown in Fig. 9, there is a positive shift of BE in the presence of an alloy, which is slightly higher in case of the most active PdZn/ZnO H_2 sample. The shift of Zn LMM peaks from low BE to higher values in the presence of the PdZn alloy was caused by the decreased negative charge on Zn. This can be attributed to a synergy between support and PdZn particles in which the electrons from Zn interact with the positively charged oxygen vacancies unquestionably present on the interface in the PdZn/ZnO H_2 sample.

The influence of the calcination atmosphere of ZnO on the chemical and electronic state of Pd species in PdZn/ZnO catalyst was analysed in detail. It was expected that the small local variation of the electronic charge concentration in the ZnO supports would influence the BE of Pd in the resulting PdZn/ZnO catalysts. In our study, careful fitting of the obtained XPS signal of Pd 3d in case of all of the catalysts studied here showed similarly the coexistence of three different Pd species. For example, a representative Pd 3d XPS spectrum of PdZn/ZnO H_2 catalyst is shown in Fig. 10. The Pd 3d region presented a doublet of Pd $3d_{5/2}$ and Pd $3d_{3/2}$ at 335.04 and 340.35 eV, which was assigned to Pd (0) species. Another doublet positioned at 335.93 and 341.29 eV can be assigned to Pd in PdZn alloy. With accordance to the literature, the bimetallic bonding with Zn produces positive BE shift in the core levels and valence d band of the group 10 metals [42]. The positive shift is connected with the reduction of electron population and subsequent shift of the valence d orbital. The remaining third doublet at 336.6 and

342.4 eV would be attributed to oxidized Pd. The presence of oxidized Pd could

be expected due to the fact that Pd easily reacts with oxygen from air at ambient conditions and the samples were not pre-reduced *in situ* before the XPS-experiment. The XPS assignment agrees well with the values reported in the literature [17,43]. The existence of Pd in the metallic state can be the result of not complete alloy formation, or the decomposition of PdZn alloy upon air exposure to Pd and Zn [43]. Additionally, the presence of separately existing metallic Pd particles on XPS spectra agrees well with our results from HRTEM image analysis of lattice spacing of single particles.

For comparison, the binding energies obtained for PdZn/ZnO COM, PdZn/ZnO air, PdZn/ZnO H_2, PdZn-ZnO O_2 are listed in Table 4. As it can be seen in this table, the XPS surface analysis showed that the surface of the investigated catalysts was composed of PdZn alloyed particles as well as separately existing Pd metallic particles dispersed on the surface of ZnO support.

The observed positive shift of binding energy (BE) of Pd 3d in PdZn/ZnO H_2 is the result of the strong synergy between the metal alloy nanoparticles and ZnO support. The increase of BE can be explained by the interaction of separately existing Pd (0) particles with local positively charged oxygen vacancies on ZnO support, resulting in the charge withdrawal from Pd metal, caus- ing the increase in BE in the core level of the metal. In addition, the binding energy of Pd in PdZn alloy is shifted to the highest value in PdZn/ZnO H_2 as compared BE of PdZn in other studied catalysts. This shift of BE suggests that the surface of PdZn alloy in the most active catalyst is the richest in Zn of all the PdZn surfaces of the studied catalysts. Noteworthy, better catalytic performance of Zn rich PdZn alloys was previously reported in MSR [17,24]. Moreover, the ratio of intensity of the photoelectron peak of Zn $2p_{3/2}$ to Pd $3d_{5/2}$ was calculated, normalised by the appropriate atomic sensitivity factors of Pd = 4.8 and Zn = 4.6 [44]. As it is listed in Table 4, the most active catalyst PdZn/ZnO H_2 as well as the least active PdZn/ZnO COM had the highest total amount of Pd exposed on the surface of the catalyst, whereas PdZn supported on ZnO calcined in oxidizing atmospheres had relatively less exposure of Pd on the surface. Taking into consideration that ZnO calcined in O_2 or air had significantly higher BET surface areas (see Table 1), it is most likely that Pd in these catalysts is encapsulated in the pores of ZnO supports. The composition of Pd 3d based on the relative intensity of Pd 3d signals was calculated and it is shown in Table 4. When comparing the catalysts activity results (see Table 2) with the catalyst compositions taken from XPS results, a clear correlation can be established between the selectivity to CO_2 of PdZn/ZnO catalysts and the extent of alloy formation. The selectivity to MSR increased proportionally to the amount of PdZn alloy formed. Interestingly, PdZn/ZnO COM with a high alloy extent (over 50%), showed the poorest activity in low temperature-MSR. On the other hand, PdZn/ZnO H_2 with very similar composition of Pd 3d peak showed the best performance regarding selectivity and activity in this reaction. Therefore, it can be concluded

that no direct correlation could be found between the extent of alloy formation and activity of the catalyst in low temperature -MSR. On the other hand, lower activity of PdZn ZnO COM generally could be associated with a much higher size of PdZn alloy. However it was previously reported that the increase in PdZn particle had no adverse effect on the activity of the catalyst in MSR [34]. Thus, the lower activity can be associated with the negative influence of the type of active sites present on the surface of ZnO COM support.

3.5. *Study of the metal–support interaction by TPR experiments*

In order to explore in more detail the interaction between metal species and ZnO supports calcined in various atmospheres, TPR experiments were conducted. The XPS study showed clearly that the electronic state of ZnO support is strongly affected by the type of gas used during its calcination. Thus, it could be anticipated that the reduction characteristics of these catalysts would also vary with the type of ZnO support or more specifically with the calcination atmosphere of the support.

The H_2-TPR profiles of the studied catalysts are displayed in Fig. 11. It should be noted that no hydrogen consumption or desorption was recorded on the pure ZnO H_2 support. This clearly indicates that in the absence of Pd, ZnO H_2 cannot be reduced below 600 °C. Surprisingly, the negative peak at low temperature commonly assigned to decomposition of PdH_x was not observed in our experiments. This low temperature peak indicates the presence of metallic Pd in the samples [34]. The presence of Pd metal was evident in the XPS results and HRTEM, so the absence of this TPR peak was rather surprising. Nevertheless, this can be explained by the fact that the hydride could be decomposed once it was formed; therefore observation of the TPR decomposition peak could be masked by a major and positive peak due to the reduction of PdO as it was reported in other studies [39]. It was noted that the reduction of all of the PdZn/ZnO catalysts started at a similar low temperature range of 51–70 °C. These TPR peaks were undoubtedly attributed to the reduction of PdO [45,46]. It should be mentioned that these reduction temperatures are generally lower than the values reported in the literature for similar catalytic systems [46,47]. This indicates that the palladium oxide in this work was present in the form of a passive thin surface layer on the well dispersed Pd particles. Interestingly, there are two overlapping peaks observed in the case of catalysts calcined in N_2, and air (the first around 60 °C and the other around 70 °C), but importantly, in the case of the former the low temperature peak is more prominent. On the other hand, in PdZn/ZnO air, a slightly higher intensity was recorded for the higher temperature peak. The difference in intensity of these peaks can be the result of the influence of the presence of O_2 during calcination of ZnO air, which is able to create special active

sites on the support. This assumption was confirmed by the TPR profile of PdZn/ZnO O2, where one peak is observed at around the same temperature of 72 °C with a small shoulder at lower temperatures. The presence of two peaks in the TPR profile suggests the co- existence of two different Pd^{2+} species with different environment and type of interaction with ZnO support. Thus, the lower temperature peak was attributed to the interface-boundary oxygen atoms on Pd which are in close vicinity to the oxygen vacancies. The reduction of PdO in these areas is promoted by strong metal–support interaction and it is influenced by the increased mobility of lattice oxygen. Thus, this peak is more intense in PdZn supported on ZnO N2 than in PdZn ZnO air. Similar observations were made in the TPR studies of Cu catalysts [47] and Ce doped with CuO [48,49]. With a strong agreement to the above conclusion, the most active catalyst (PdZn/ZnO H2) shows a broad peak at a lower temperature (58 °C), suggesting the presence of the active sites in the close proximity to the defected ZnO sites. In addition, as it could be anticipated from other results, PdZn COM showed a single very sharp peak at a higher temperature (68 °C), indicating one type of PdO present on this catalyst, possibly supported on stoichiometric ZnO. In addition, there is a very broad peak visible in temperatures above 250 °C in all of catalysts studied, which represents a continuous PdZn alloy formation [4]. The dissociation of molecular hydrogen on the surface of Pd metal provides very active atomic hydrogen which reduces ZnO by abstracting O^{2-} from its surface. Overall, the presence of oxygen vacancies is apparent in TPR results, leading to a significant decrease in the reduction temperature of the neighboring PdO. Noteworthy, a decrease in the reduction temperature of the metal oxide supported on redox-active oxide such as ZnO is a reliable sign of the established strong metal support interaction (SMSI) [26]. It is clear that the calcination atmosphere of ZnO influences the reduction profile of the PdZn/ZnO catalysts. In summary, the TPR results agreed well with the XPS findings and also points at existence of metallic Pd particles along with PdZn alloyed particles on the surface of ZnO.

3.6. DRIFT study of CO adsorption on PdZn/ZnO catalysts

CO-adsorption-DRIFT analysis presents a unique tool to probe the chemical nature of the adsorption sites on the catalyst surface. This is because the bonding of CO to the metal is sensitive to the oxidation and coordination of the catalytically active sites. Thus, the position of the CO adsorption band on a given metal depends on the oxidation state of a metal site, nature of exposed faces and the particle size [50]. It is clear that the existence of different active sites/ensembles on PdZn/ZnO catalyst may lead to pronounced differences in its performance in low temperature-MSR. Thus, DRIFT spectra using CO as a probe molecule were

recorded at room temperature in the region of 2200–1900 cm^{-1} for representative PdZn/ZnO catalysts. The resulting DRIFT spectra are presented in Fig. 12. The spectra were recorded in the increasing CO exposure time from spectra 1 freshly reduced catalyst to spectra to spectra three, four-fully saturated sample.

All the DRIFT results showed the coordination bands of CO in two regions. CO adsorbed in bridging mode (1981–1960 cm^{-1}) on the Pd (0) and CO adsorption on the steps and edges of rows of Pd in PdZn in linear (a-top) mode (2093–2010 cm^{-1}) [51] [52]. The modes of adsorption are schematically shown in Fig. 12.A. The bands with a wavenumber higher than 2150 cm^{-1} can be assigned to CO in gas phase [52]. As it can be seen from this study, the type of ZnO substrate affects the vibrational frequency of adsorbed CO. The presence of the bridging mode is the result of ensemble of neighboring Pd atoms on the surface of all the catalysts. This confirms the previous results from the catalysts composition obtained in TPR, XPS and HRTEM studies. The CO adsorbs mostly in bridging mode on PdZn/ZnO N_2 and PdZn/ZnO O_2. This finding agrees well with the XPS results that showed lower alloy formation in PdZn/ZnO O_2 sample as compared with PdZn/ZnO COM. Thus, due to higher alloy extent present in PdZn/ZnO COM, CO adsorbed mainly in linear mode on this sample (see Fig. 12 D). Moreover, higher concentration of CO linearly bonded to Pd was found on the samples with higher concentration of Zn on the surface [52]. Taking into consideration the size of the PdZn nanoparticles, it can be concluded that CO adsorbs mostly in bridging mode on the smaller PdZn particles. On the most active catalyst, PdZn/ZnO H_2 there is also two adsorption modes present. Careful analysis of the wavenumbers revealed that there is a blueshift of bridging mode on the PdZn/ZnO H_2 (1975.58 cm^{-1}) and linear mode (2075.1 cm^{-1}) as compared to the bridging mode (1979.1 cm^{-1}) and linear mode (2087 cm^{-1}) on PdZn/ZnO O_2 or bridging (1981.1 cm^{-1}) and linear (2100 cm^{-1}) on PdZn/ZnO N_2. This shift of wavenumber to lower values can be ascribed to the electronic interaction between Pd and ZnO support. The presence of free electrons from oxygen vacancies in ZnO increases the charge of Pd. In general, higher elec- tron density of metal increases the back-donation to $2\pi^*$ orbitals of adsorbed CO which in turn makes the adsorption weaker and shifted to lower frequencies [36]. The presence of free electrons associated with the vacancies on ZnO support in PdZn/ZnO H_2 sample was previously confirmed by TPR and XPS results in the present work.

Moreover, limited stability of the PdZn surface alloy in all of the samples was observed with a prolonged exposure to CO atmosphere. As it can be seen in Fig. 12, there was a redshift observed with increasing time in CO atmosphere. The saturated spectra numbers three and four on each of the samples in this figure

closely resembled that of CO adsorbed on Pd metal. This result strongly indicates that there are some homogenous structural changes taking place on the surface of the studied catalysts. With increasing time, new surface sites are created on these catalysts which are probably Pd rich. Since interaction of CO with Pd sites is much stronger than its interaction with Zn containing sites [36] it can be assumed that as a result of the strong interaction with CO, the Pd atoms in PdZn bulk alloy segregate to the surface. Similar observations were described by other authors [53], however in our case changes of observed intensity of the bands were only noted in case of PdZn/ZnO H2 sample. The most active catalyst showed redshift of the frequencies accompanied by increased intensity of bridging mode with exposure time. In this case, the surface reconstruction step might be affected by the presence of free electrons on the sur- face of ZnO support, which can give rise to the production of new active sites on the surface. Therefore, it is very likely that the PdZn alloys on these supports could be prone to segregation of Pd to the surface of the catalyst. The results of CO–DRIFT analysis suggested that the stability of these catalysts under methanol steam reforming conditions could be limited. Therefore, the stability of the representative catalyst PdZn ZnO H2 was tested under methanol steam reforming conditions for a period of 48 h and the result is depicted in Supplementary material, Fig. s1. A total drop of conversion of 24% was recorded, which is slightly higher than the values reported in the literature for the similar system [54]. This very interesting result can be undoubtedly attributed to the restructuring changes of the sur- face of PdZn/ZnO catalyst under MSR conditions. The instability of this catalytic system will be studied in more detail in our future work.

4. Conclusions

The obtained results clearly identify that strong synergism between active sites present on intermetallic PdZn alloy and active sites present ZnO support is necessary to obtain excellent catalytic performance of PdZn/ZnO systems in methanol steam reforming. The XPS study showed that the composition of the surface of the studied catalysts contained a mixture of Pd metallic and PdZn alloyed particles supported on ZnO. It should be noted that the amount of Pd metallic present on the surface of the studied catalysts as calculated from XPS experiments was very similar in case of all the materials studied. Therefore, it can be concluded that the presence of these particles had no adverse effects on the catalysts performance, which agrees well with the literature findings [35]. Indeed, the activity of these monometallic Pd particles is altered by the presence of the ZnO support, favoring higher production of CO_2 over CO.

The influence of the calcination atmosphere of the ZnO precursor on the performance of PdZn/ZnO catalyst in low temperature MSR was studied in detail and a very active and ultraselective catalyst was obtained by supporting

Pd on ZnO calcined in H_2. The activity of the PdZn catalyst was found to be independent of the extent of the PdZn alloy formed. However, higher selectivities to CO_2 were achieved by the samples showing higher amount of PdZn alloy on the surface as evidenced by XPS results. The extent of alloy formation was found to be influenced by the BET surface area and ZnO supports with higher BET values displayed lower extent of alloy formation. A direct correlation was found for the first time between the catalytic performance of PdZn/ZnO catalysts in low tempera- ture MSR and the calcination atmosphere of the ZnO support. Thus, the performance of the catalysts increased from PdZn supported on ZnO calcined in oxidative atmospheres to PdZn/ZnO calcined in nitrogen and was the best in case of PdZn supported on ZnO calcined in H_2. The exceptional performance in low temperature MSR of PdZn/ZnO H_2 catalyst was attributed to the presence of higher concentration of oxygen vacancies in ZnO H_2, as evidenced by TPR, XPS and CO-DRIFT studies. The gathered results showed that the activity of PdZn catalyst is strongly affected by the morphology and crystallinity of the ZnO support which governs the type of specific active sites responsible mainly for water activation. The stronger synergy between Pd and ZnO was achieved in the presence of oxy- gen vacancies in ZnO support, which resulted in the high selectivity towards MSR of the best catalyst. Thus, a clear correlation was dis- covered for the first time between the amount of oxygen defects present on the ZnO support as indicated by XPS, TPR, CO-DRIFT studies and the activity of PdZn/ZnO catalysts. Unfortunately, the PdZn alloy in these systems was found to be unstable under pro- longed CO exposure during DRIFT experiments. The stability test carried out under methanol steam reforming conditions showed a 24% drop in conversion of the most active catalyst during 48 h on stream. Thus, it was confirmed that surface reconstruction is likely to take place during the MSR reaction, possibly involving either segregation of Pd to the surface from the bulk of the PdZn alloy, or other changes in the composition of the PdZn alloy due to reorder- ing under reaction conditions. Further research is currently carried out to understand the mechanism of deactivation of these catalytic systems.

To sum up, it is expected that the presented results would aid in the rational design of more active and selective catalyst for application at even lower temperature (170 °C) for hydrogen production by MSR.

Acknowledgement

The research leading to these results has received funding from European Union' Seventh Framework Programme (FP7/2007-2013) for the Fuel Cells and Hydrogen Joint Technology Initiative under grant agreement number 303476 10 (BeingEnergy). K.Eblagon is grateful for the financial support from FCT

postdoctoral grant (PTDC/CTM/108454/2008) co-financed by FEDER and POFC and PTDC/EQU-EQU/104217/2008. The work of H.Silva was supported by FCT, grant SFRH/BD/45890/2008. Mr. F. Eblagon and Dr L. Brandão are acknowledged for fruitful discussions of the data. Dr L. Jorda Moret from ITQ-Universidad Politecnica de Valencia is thanked for performing the XRD study of PdZn alloy formation. Authors are also grateful to Dr M. Reinikainen and Dr S. Pekka from VTT Technical Research Centre of Finland for performing TPR mea- surements. Mr. P. Ribeirinha from FEUP is thanked for performing the stability tests and Dr. P.J.F.Harris is acknowledged for performing additional HRTEM characterization.

Appendix A. Supplementary data

Supplementary data associated with this article can be found, in the online version, at http://dx.doi.org/10.1016/j.apcatb.2014. 02.032.

References

[1] M.U. Niemann, S.S. Srinivasan, A.R. Phani, A. Kumar, D.Y. Goswami, E.K. Ste- fanakos, J. Nanomater. 2008 (2008) 1–9.
[2] B. Lindström, L.J. Pettersson, P.G. Menon, Appl. Catal. A 234 (2002) 11–125.
[3] Y.-H.P. Zhang, J.-H. Xu, J.-J. Zhong, Int. J. Energy. Res. 37 (2013) 769–779.
[4] N. Iwansa, M. Yokoshikawa, W. Nomura, M. Arai, Appl. Catal. A 292 (2005) 215–222.
[5] G.A. Olah, Angew. Chem. Int. Ed. 44 (2005) 2636–2639.
[6] S. Kim, M. Kang, J. Ind. Eng. Chem. 18 (2012) 969–978.
[7] D.R. Palo, Chem. Rev. 107 (2007) 3992–42021.
[8] P. Bichon, M. Asheim, A. Jordal, T. Sperle, M. Fathi, A. Holmen, E.A. Blekkan, Int. J. Hydrogen Energy 32 (2007) 1799–1805.
[9] J.-P. Shen, C. Song, Catal. Today 77 (2002) 89–98.
[10] C.E. Taylor, B.H. Howard, C.R. Myers, Ind. Eng. Chem. Res. 46 (2007) 8906–8909.
[11] O. Llinich, Y. Liu, C. Castellano, G. Koermer, A. Moini, R. Farrauto, Platinum Met. Rev. 52 (2008) 134–143.
[12] K.M.K. Yu, W. Tong, A. West, K. Cheung, T. Li, G. Smith, Y. Guo, S.C. Tsang, Nat. Commun. 3 (2012) 1–7.
[13] S. Sá, H. Silva, L. Brandão, J.M. Sousa, A. Mendes, Appl. Catal. B 99 (2010) 43–57.
[14] M.-C. Tsai, J.-H. Wang, C.-C. Shen, C.-T. Yeh, J. Catal. 279 (2011) 241–245.
[15] Y. Matsumura, H. Ishibe, J. Mol. Catal. A 345 (2011) 44–53.

[16] N. Iwasa, S. Kudo, H. Takahashi, S. Masuda, N. Takezawa, Catal. Lett. 19 (1993) 211–216.
[17] M. Friedrich, D. Teshner, A. Knop-Gericke, M. Armbruster, J. Catal. 285 (2012) 41–47.
[18] Y. Usami, K. Kagawa, M. Kawazoe, Y. Matsumura, Appl. Catal. A 171 (1998) 123–130.
[19] N. Iwasa, N. Takezawa, Top. Catal. 22 (2003) 215–224.
[20] M. Friedrich, S. Penner, M. Heggen, M. Armbruster, Angew. Chem. Int. Ed. 52 (2013) 4389–4392.
[21] F. Liao, Y. Huang, J. Ge, W. Zheng, K. Tedsree, P. Collier, X. Hong, S.C. Tsang, Angew. Chem. Int. Ed. 50 (2011) 2162–2165.
[22] E. Jeroro, J.M. Vohs, J. Am. Chem. Soc. 130 (2008) 10199–10207.
[23] H. Lorenz, C. Rameshan, T. Bielz, N. Memmel, W. Stadlmayr, L. Mayr, Q. Zhao, S. Soisuwan, B. Klötze, Chem. Catal. Chem. 5 (2013) 1273–1285.
[24] J. Strunk, K. Kahler, X. Xia, M. Muhler, Surf. Sci. 603 (2009) 1776–1783.
[25] B. Halevi, S. Lin, A. Roy, H. Zhang, E. Jeroro, J. Vohs, Y. Wang, H. Guo, J. Phys. Chem. C 117 (2013) 6493–6503.
[26] N. Acerbi, S.C.E. Tsang, G. Jones, S. Golunski, P. Collier, Angew. Chem. Int. Ed. 52 (2013) 1–6.
[27] G. Xiong, L. Luo, C. Li, X. Yang, Energy Fuels 23 (2009) 1342–1346.
[28] M. Arsalanfar, A.A. Mirzaei, H.R. Bozorgzadeh, J. Nat. Gas Sci. Eng. 6 (2012) 1–13.
[29] M.Y. Ge, H.P. Wu, L. Niu, J.F. Liu, S.Y. Chen, P.Y. Shen, Y.W. Zeng, J. Cryst. Growth 305 (2007) 162–166.
[30] J. Kiss, A. Witt, B. Meyer, D. Marx, J. Chem. Phys. 130 (2009) 184706–184720.
[31] G.R. Li, T. Hu, G.L. Pan, T.Y. Yan, X.P. Gao, H.Y. Zhu, J. Phys. Chem. C 112 (2008) 11859–11864.
[32] A. Mclaren, T. Valdes-Solis, G. Li, S.C. Tsang, J. Am. Chem. Soc. 131 (2009) 12540–12541.
[33] C. Shao, L. Tu, A. Yu, B. Li, X. Zhou, Thin Solid Films 525 (2012) 148–153.
[34] W. Yanhua, Z. Jingchang, X. Hengyong, B. Xuefeng, Chin. J. Catal. 28 (2007) 234–238.
[35] A. Karim, T. Conant, A. Datye, J. Catal. 243 (2006) 420–427.
[36] I. Eswaramoorthi, A.K. Dalai, Int. J. Hydrogen Energy 34 (2009) 2580–2590.
[37] S. Du, Y. Tian, H. Liu, J. Liu, Y. Chen, J. Am. Ceram. Soc. 89 (2006) 2440–2443.
[38] P.T. Hsieh, Y.C. Chen, K.S. Kao, C.M. Wang, Appl. Phys. A 90 (2008) 317–321.
[39] M.L. Cubeiro, J.L.G. Fierro, Appl. Catal. A: Gen. 168 (1998) 307–322.
[40] M. Chen, X. Wang, Y.H. Yu, Z.L. Pei, X.D. Bai, C. Sun, R.F. Huang, L.S.

Wen, Appl. Surf. Sci. (2000) 134–140.
A. M. Leonarda, E. Moretti, L. Storaro, P. Patrono, F. Pinari, E. Rodriguez-Castellon, Jimenez-Lopez, G. Busca, E. Finocchio, T. Montanari, R. Frattini, Appl. Catal. 312 (2006) 220–228.
[41] J.A. Rodriguez, M. Kuhn, J. Phys. Chem. 100 (1996) 381–389.
[42] V. Engels, D.A. Jefferson, F. Benaskar, P.C. Thune, A. Berenguer-Murcia, B.F.G. Johnson, A.E.H. Wheatley, Nanot 22 (2011) 205701–205721.
[43] http://www.cem.msu.edu [Online].
[44] P. Pfeifer, K. Schubert, M.A. Liauw, G. Emig, Appl. Catal., A 270 (2004) 165–175.
[45] Y.-H. Chin, R. Dagle, J. Hu, A.C. Dohnalkova, Y. Wang, Catal. Today 77 (2002) 79–88.
[47] L. Yang, G.-D. Lin, H.-B. Zhang, Appl. Catal., A 455 (2013) 137–144.
[48] S. Patel, K.K. Pant, Fuel Process. Technol. 88 (2007) 825–832.
[49] A. Aranda, S. Agouram, J.M. López, A.M. Mastral, D.R. Sellick, B. Solsona, S.H. Taylor, T. García, Appl. Catal., B 127 (2012) 77–88.
[50] S. Royer, D. Duprez, Chem. Catal. Chem. 3 (2011) 24–65.
[51] W. Stadlmayr, C. Rameshan, C. Weilach, H. Lorenz, M. Hävecker, R. Blume, T. Rocha, D. Teschner, A. Knop-Gericke, D. Zemlyanov, S. Penner, R. Schlögl, G. Rupprechter, B. Klötzer, N. Memmel, J. Phys. Chem. C 114 (2010) 10850–10856.
[52] L. Bollmann, J.L. Ratts, A.M. Joshi, W.D. Williams, J. Pazmino, Y.V. Joshi, J.T. Miller, J. Catal. 257 (2008) 43–54.
[53] K. Föttinger, Catal. Today 208 (2013) 106–112.
[54] T. Conant, A.M. Karim, V. Lebarbier, Y. Wang, F. Girgsdies, R. Schlögl, A. Datye, J. Catal. 257 (2008) 64–70.

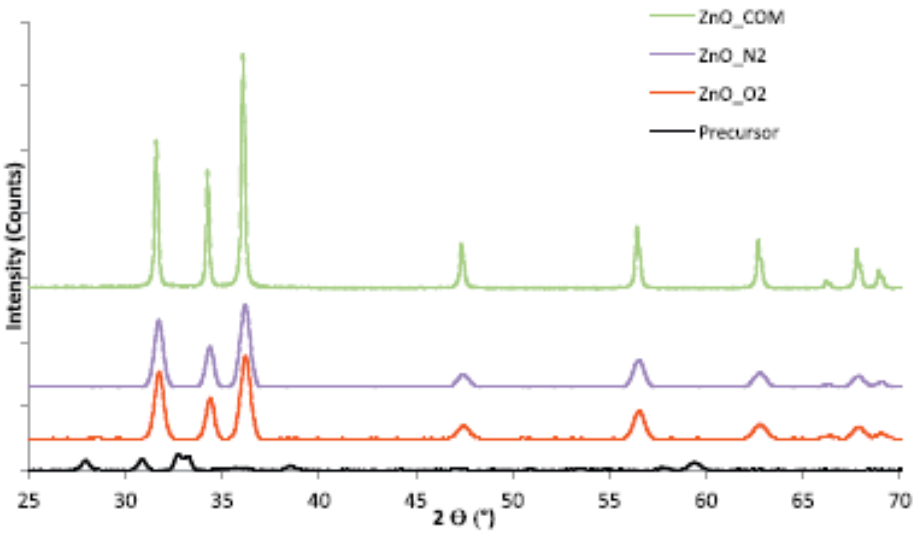

Fig. 1. XRD pattern of $Zn_4CO_3(OH)_6{\cdot}H_2O$ (precursor), ZnO calcined in N_2 (ZnO_N_2), ZnO calcined in O_2 (ZnO_O_2) and ZnO commercial (ZnO_COM).

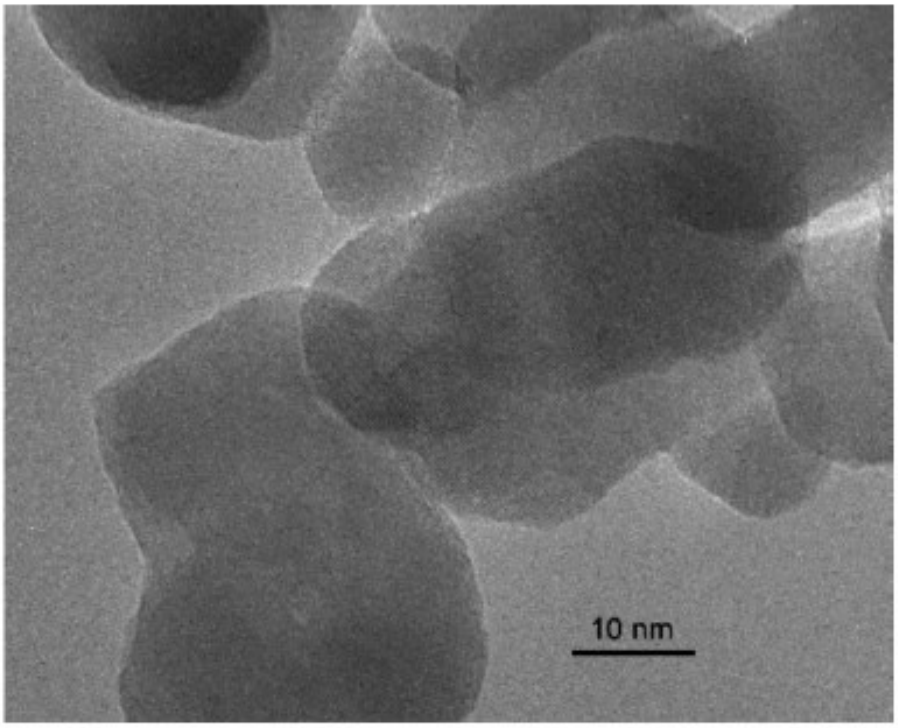

A

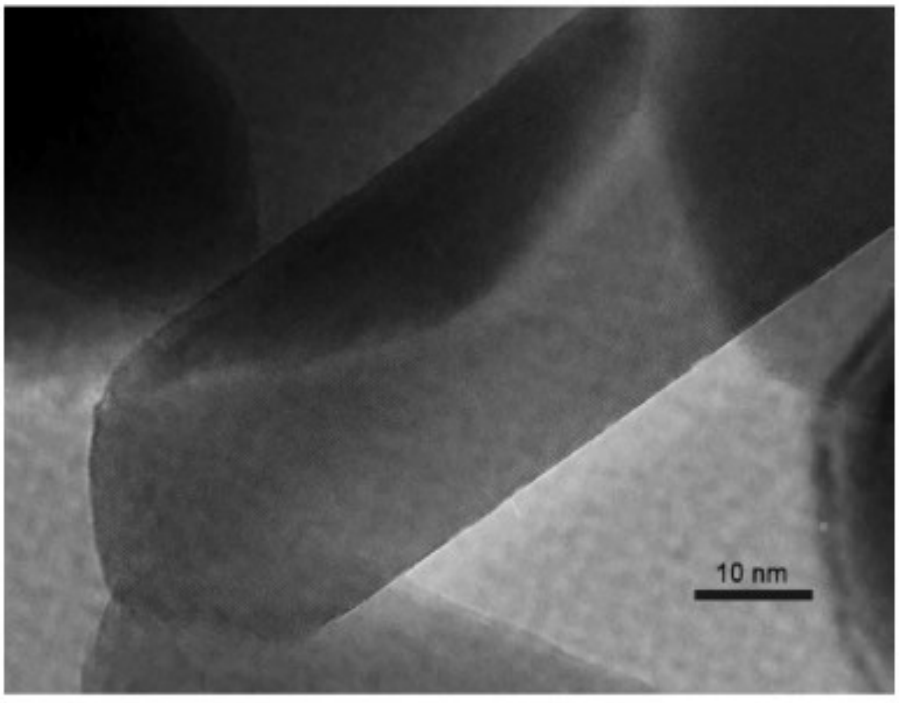

B

Fig. 2. HRTEM micrographs of A) ZnO_H_2 and B) ZnO_COM.

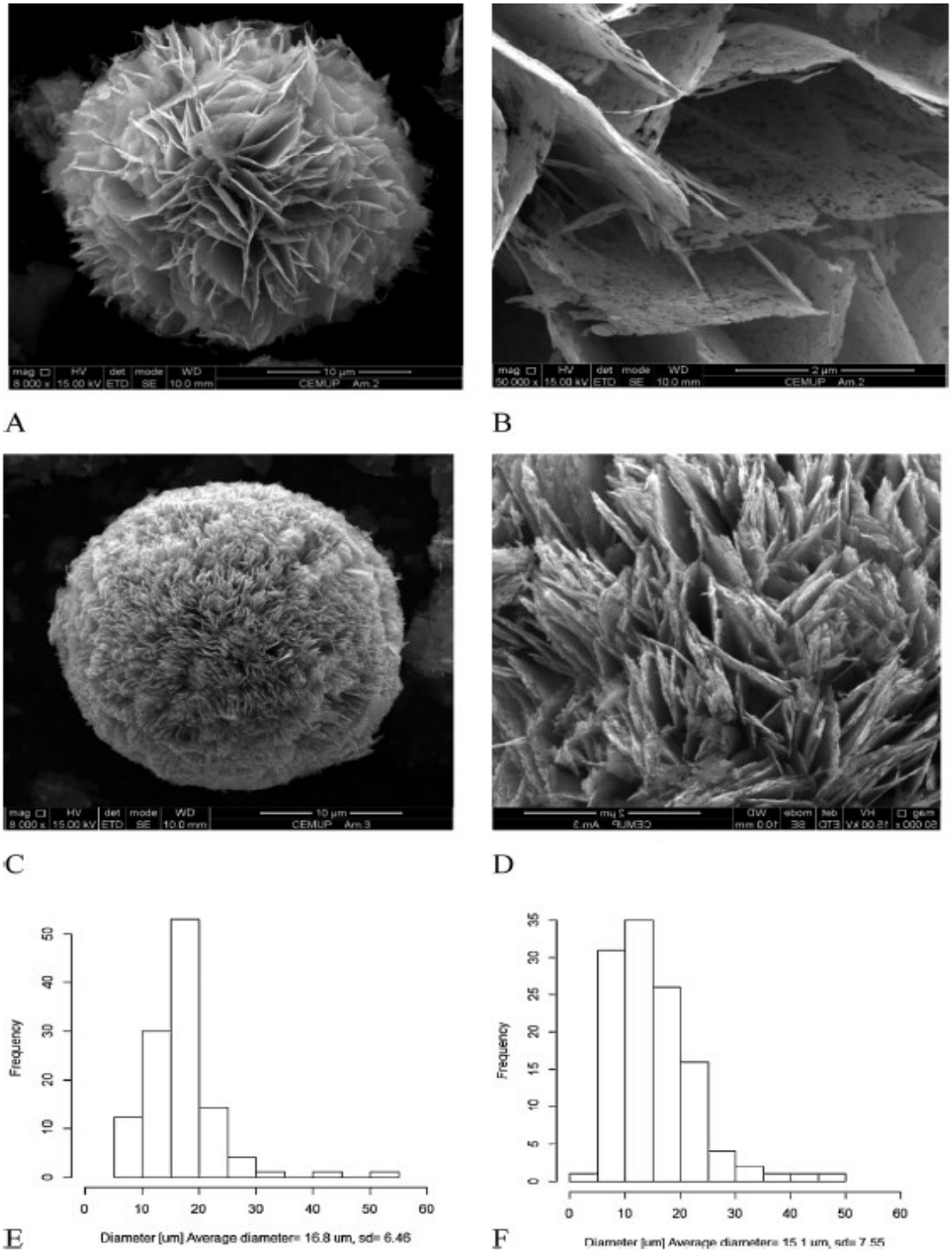

Fig. 3. SEM images of the ZnO particles prepared by calcination in different atmospheres. A-ZnO_O_2, B-close-up of ZnO_O_2, C-ZnO_H_2, D-close-up of ZnO_H_2, E)-particle size distribution of ZnO_O_2, F) particle size distribution of ZnO_H_2.

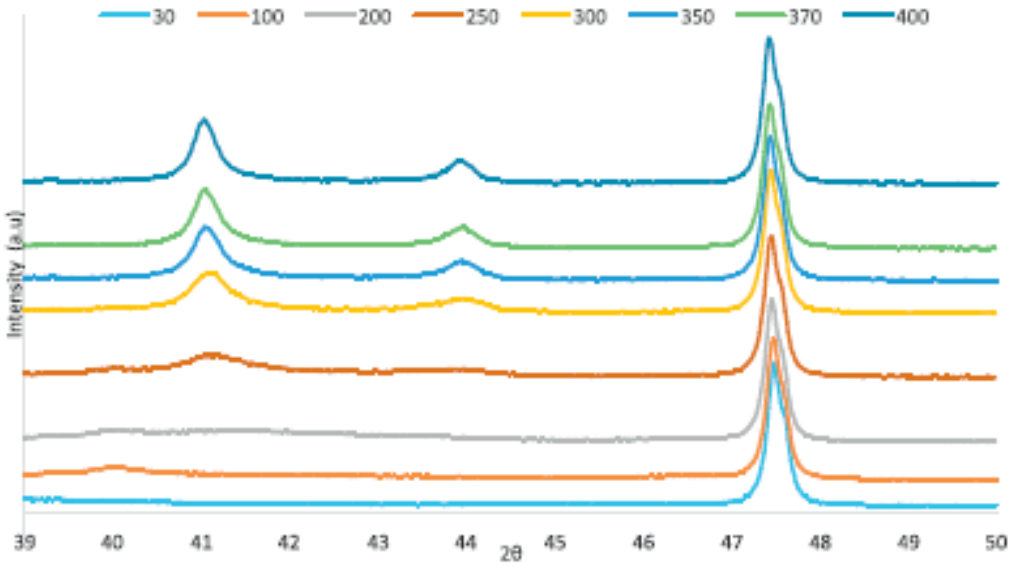

Fig. 4. XRD pattern obtained during reduction of PdZn_ZnO_COM at various temperatures (°C). Large peak at 2θ = 47.7° is ascribed to ZnO (1 0 2) plane [29].

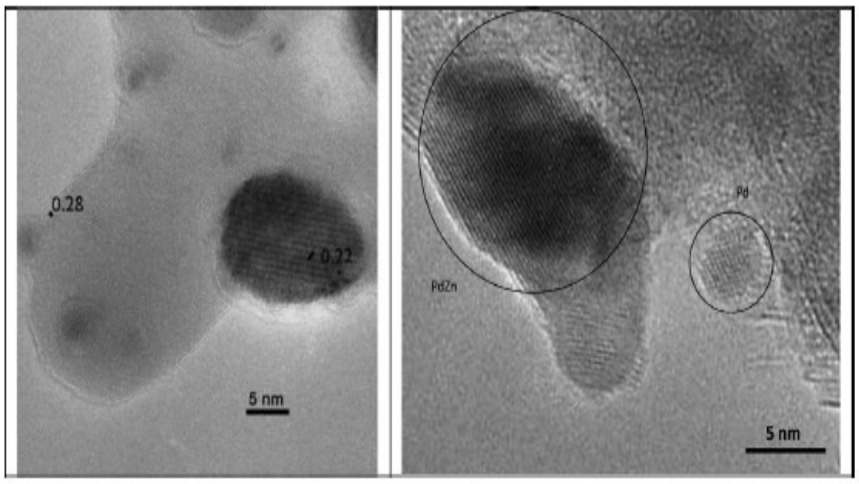

Fig. 5. Left: HRTEM image of a single polycrystalline PdZn particle supported on ZnO_H2. The lattice fringes of PdZn (1 0 1) and ZnO (1 0 0) are marked. Right: HRTEM image of single PdZn and Pd particles supported on ZnO_COM.

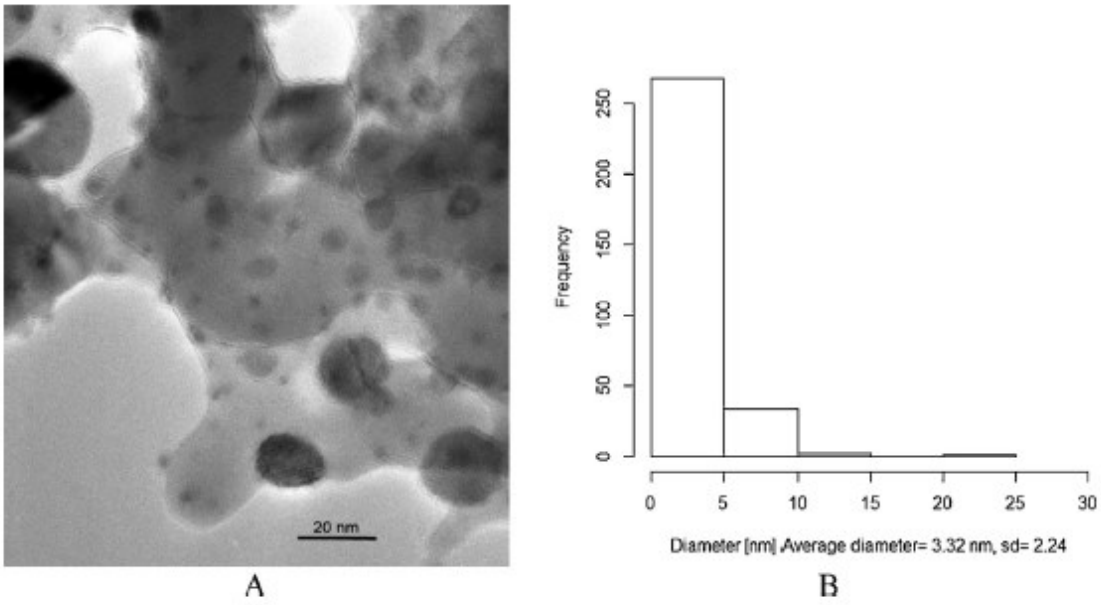

Fig. 6. (A) HRTEM image of PdZn/ZnO_H_2. (B) Particle size distribution of the same sample.

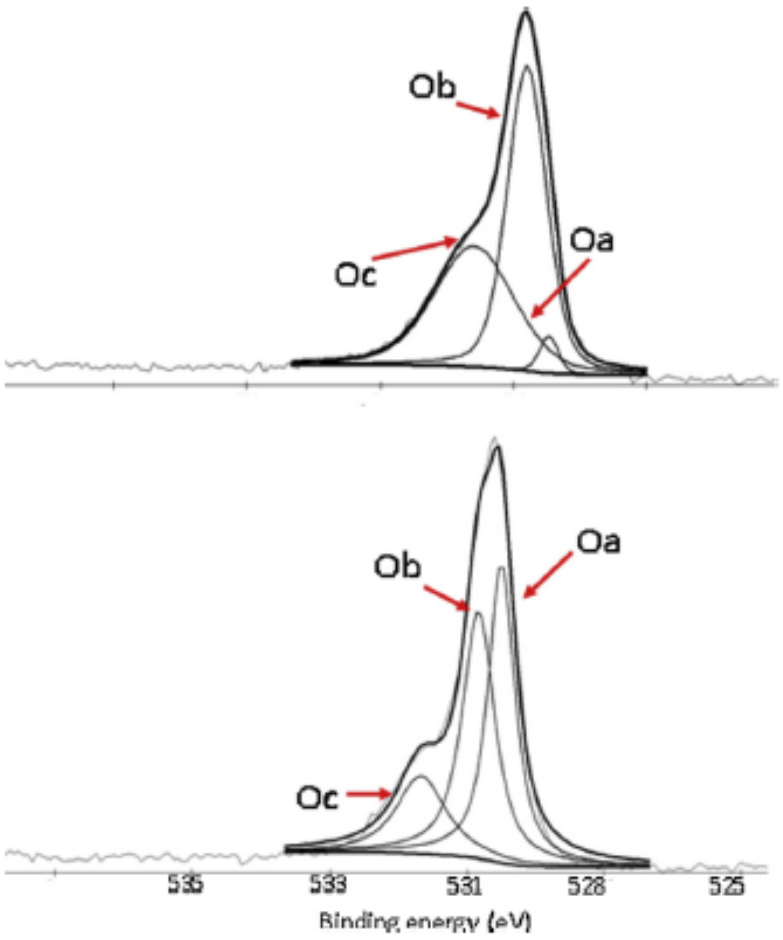

Fig. 7. Comparison of the O 1s spectra of PdZn_ZnO_H_2 (top) and PdZn_ZnO_O_2 (bottom) with the assigned peaks from various oxygen species.

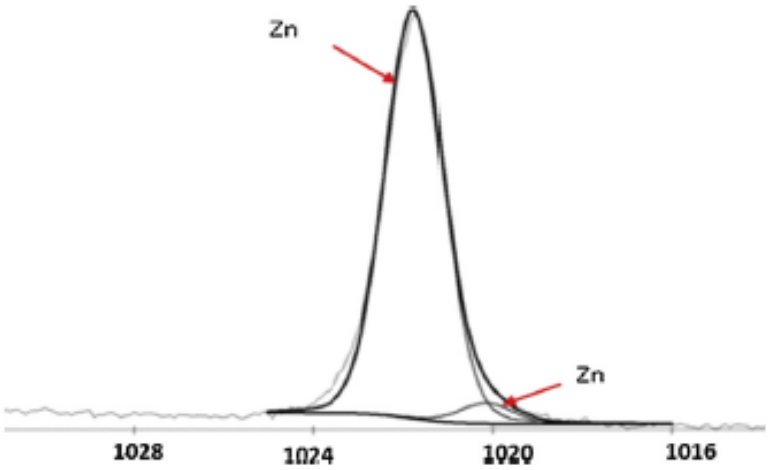

Fig. 8. Representative highly resolved core level Zn $2p_{3/2}$ spectrum of PdZn_ZnO_COM.

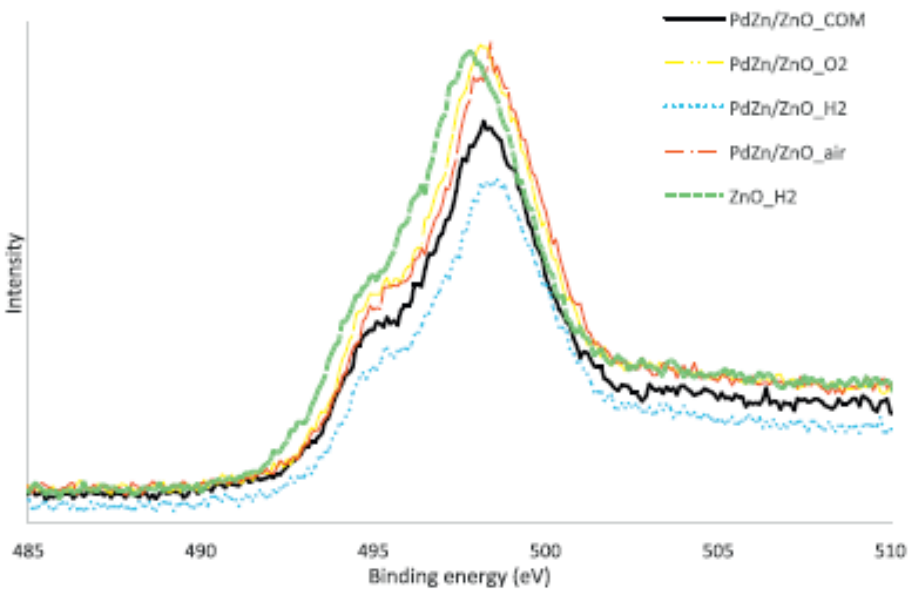

Fig. 9. The Zn LMM line of PdZn/ZnO catalysts as compared to pure ZnO_H_2_support.

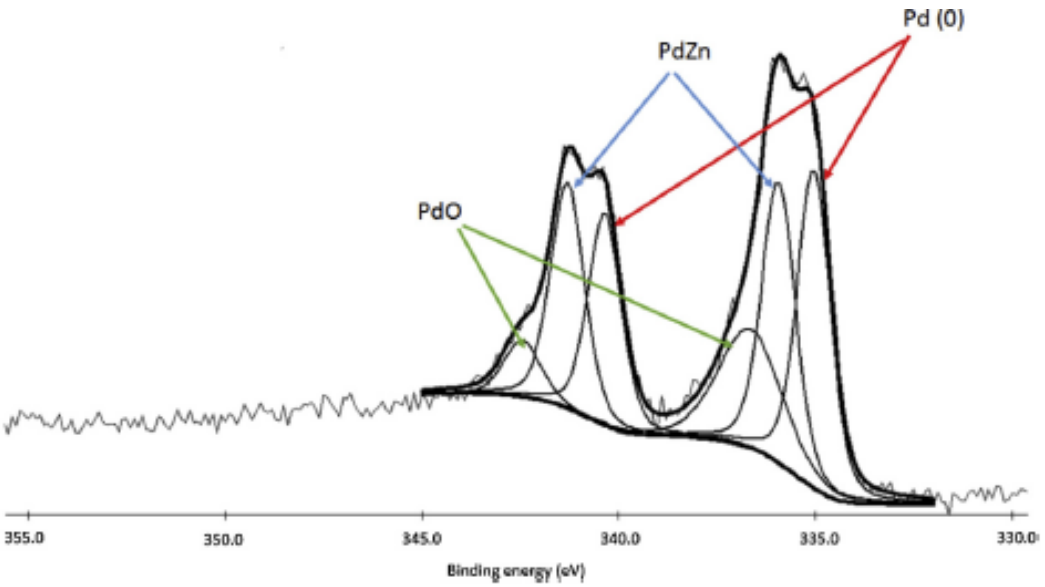

Fig. 10. Representative XPS spectra of the elemental peaks of Pd 3d in PdZn/ZnO_H_2

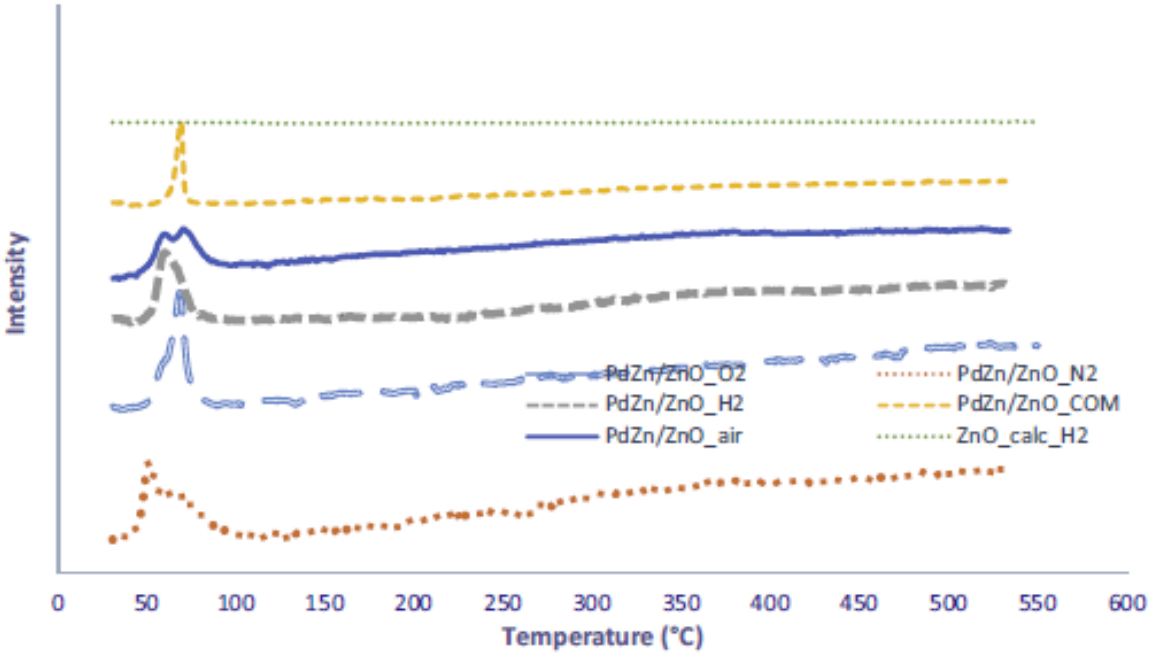

Fig. 11. H_2-TPR profile of ZnO_H_2 and PdZn/ZnO catalysts.

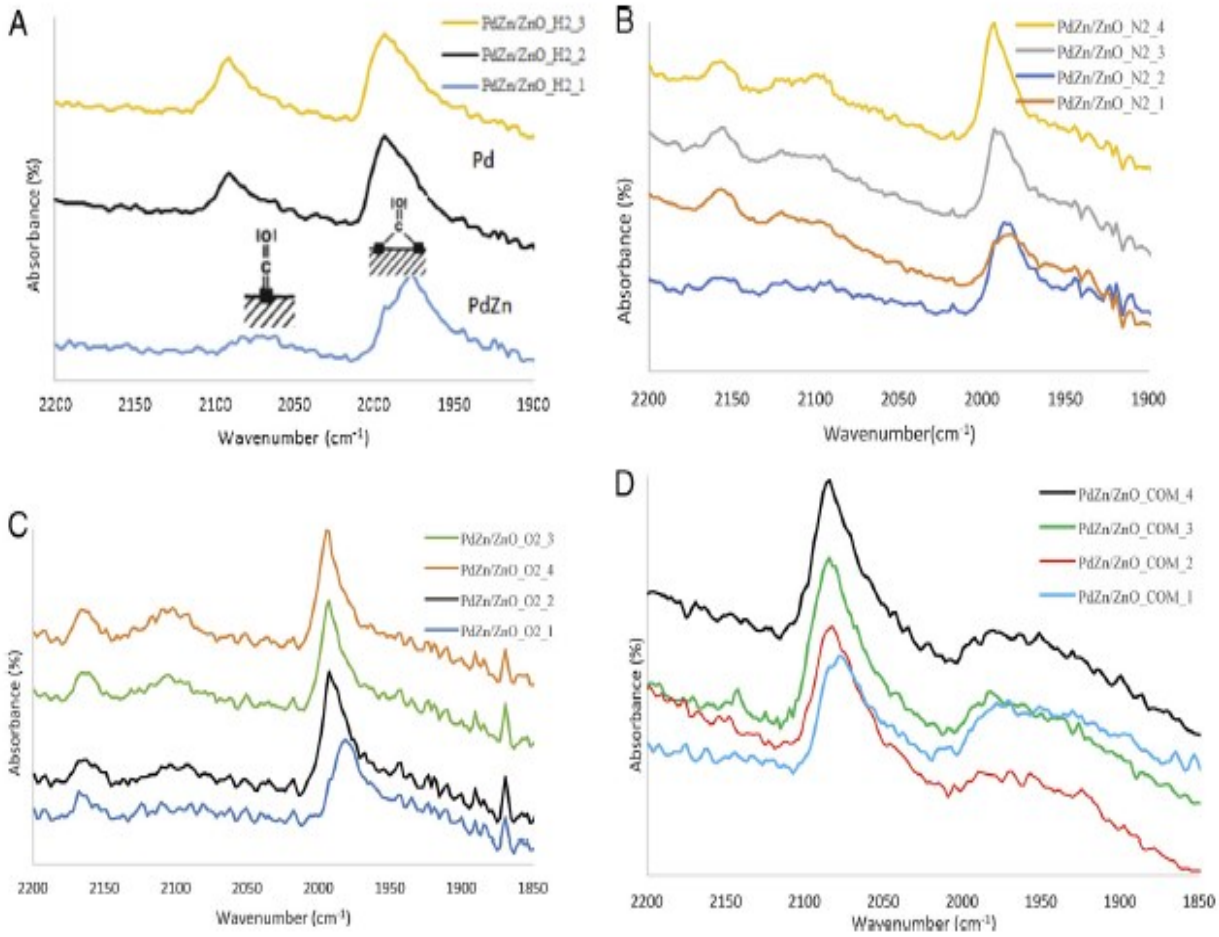

Fig. 12. CO adsorption at room temperature on (A) PdZn/ZnO H2, (B) PdZn/ZnO N2, (C) PdZn/ZnO O2and (D) PdZn/ZnO COM. Spectra 1–4 were recorded with increasing time of CO exposure.

Table 1
The physicochemical characterization of the ZnO supports studied.

Sample	BET surface area (m^2/g)	Ratio (1 0 0)/(0 0 2)
ZnO_O_2	88	1.59
ZnO_air	76	1.56
ZnO_N_2	27	1.13
ZnO_H_2	24	1.3
PdZn_ZnO_COM	16	1.2

Table 2
Catalytic performance of a series of PdZn/ZnO catalyst in low temperature MSR together with corresponding particle size measured from HRTEM images.

Sample	Activity ($\mu mol/g_{met}$ s)	CO concentration (ppm)	HRTEM particle size (nm)
PdZn_FEUP_O_2	42.6	1450	3.3
PdZn_FEUP_air	46.8	1400	2.4
PdZn_FEUP_N_2	63.8	700	2.1
PdZn_FEUP_H_2	**87.9**	**146**	**3.3**
PdZn_ZnO_COM	38.3	309	8.1

Table 3
BE and relative intensities of components of O 1s XPS spectra.

Sample	Oa BE (eV)	%	Ob BE (eV)	%	Oc BE (eV)	%
PdZn_ZnO_H_2	530.2	4.6	530.7	52	531.9	43.4
ZnO_H_2	529.8	5.9	530.2	53	531.7	40.7
PdZn_ZnO_O_2	530.2	40.5	530.8	40.2	532.0	19.2
PdZn_ZnO_COM	530.4	66	531.6	11	532.3	23
PdZn_ZnO_air	530.5	58	531.1	19	532.1	22

Table 4
BE and composition of Pd 3d XPS spectra of studied PdZn/ZnO catalysts.

Sample	BE (eV) Pd $3d_{5/2}$	BE (eV) PdZn	BE (eV) PdO	Pd 3d/Zn 2p	Composition (%) Pd/PdZn/PdO
PdZn/ZnO_COM	334.75	335.64	337.11	0.1	34/56/9
PdZn/ZnO_air	334.88	335.58	336.61	0.06	39/38/22
PdZn/ZnO_H_2	335.04	335.93	336.66	0.12	29/51/19
PdZn/ZnO_O_2	334.89	335.70	336.73	0.07	31/36/32